Supplemental Information for

Electrochemical Flow Cell Enabling *Operando* Probing of Electrocatalyst Surfaces By X-Ray Spectroscopy and Diffraction

Maryam Farmand[1,2]†, Alan T. Landers[3,4]†, John C. Lin[4,5], Jeremy T. Feaster[4,5,6], Jeffrey W. Beeman[1], Yifan Ye[1,2], Ezra L. Clark[7], Drew Higgins[4,5], Junko Yano[8], Ryan C. Davis[9]*, Apurva Mehta[9]*, Thomas F. Jaramillo[4,5]*, Christopher Hahn[4,5]*, Walter S. Drisdell[1,2]*

[1]Joint Center for Artificial Photosynthesis, Lawrence Berkeley National Laboratory, Berkeley, CA 94720, USA

[2]Chemical Sciences Division, Lawrence Berkeley National Laboratory, Berkeley, CA 94720, USA

[3]Department of Chemistry, Stanford University, Stanford, CA 94305, USA

[4]SUNCAT Center for Interface Science and Catalysis, SLAC National Accelerator Laboratory, Menlo Park, CA 94025, USA

[5]Department of Chemical Engineering, Stanford University, Stanford, CA 94305, USA

[6]Materials Science Division, Lawrence Livermore National Laboratory, Livermore, CA 94550, USA

[7]Chemical and Biomolecular Engineering Department, University of California Berkeley, Berkeley, CA 94720, USA

[8]Molecular Biophysics and Integrated Bioimaging Division, Lawrence Berkeley National Laboratory, Berkeley, CA 94720, USA

[9]Stanford Synchrotron Radiation Lightsource, SLAC National Accelerator Laboratory, Menlo Park, CA 94025, USA

†These authors contributed equally to this work.

Experimental Methods

Sample Preparation:

Cu thin films were prepared via physical vapor deposition (PVD) inside a Temescal BJD-1800 evaporator as described previously.[1] Using an electron beam, 3 nm of Cr was deposited onto degenerately-doped n^+ Si(100) wafers as an adhesion layer. Then, 100 nm of Cu was deposited onto the Cr adhesion layer. Films deposited from this instrument have been shown to have RMS roughness values between 1 and 2 nm, suitably smooth for grazing incidence measurements.[2]

Cell assembly:

After deposition of the samples, they were mounted in the electrochemical cells. The 3D-printed cell bodies are composed of proprietary urethane oligomers mixed with ethoxylated bisphenol A diacrylate and tripropyleneglycol diacrylate and were demonstrated to be stable in 0.1 M potassium carbonate buffer solution through immersion testing. A 40-gauge copper wire was stripped to create a pre-tinned end to the wire, then coiled very tightly and bent into a shape such that the coil of pre-tinned wire rested flat against the back of the Si substrate. The sample was positioned with the Cu thin film side down in a curved high-density polyethylene dish, to minimize contact with unclean surfaces. The remainder of the Cu wire was directed vertically away from the coil. A diamond scribe was used to slightly roughen a central "dot" on the backside of the Si substrate prior to fixing the wire. A small spot of In-Ga eutectic was then applied to the roughened area. The pre-bent wire was placed directly into the InGa spot and affixed onto the Si substrate using 5-min epoxy (Hardman). The epoxy cured in air for 1 h at ambient temperature.

The sample/wire assembly, which will act as the working electrode, was then threaded into the feed-through hole and lowered near the recessed well portion of the cell. Five-minute epoxy was used to fill the well before drawing the sample into the cell using the (now bottom-extruding) wire. The epoxy acts to seal the sample edges and prevent electrolyte from physically contacting the back contact of the electrode. The sample wire that extended out of the bottom of the cell was then weighted with a 5 g mass, which pulled the sample flat into the well and provided good contact with the epoxy. The epoxy cured

over one hour in this configuration. Two 50 μm diameter counter electrode Pt wires (Alfa Aesar, 99.99%) were placed into the grooves in the cell above the liquid channels and working electrode, then epoxied on the ends. The contacts for the working and counter electrodes were also epoxied into place. To "cap" the cell, a 25 μm thick sheet of polyimide film was cut to size and roughened along all edges using 600 grit SiC abrasive paper. The film was then cleaned in an ultrasonic bath of DI water and Alconox detergent, followed by a final DI water rinse and Nitrogen blow-dry. Once prepared in this way, the film was then placed over the working and counter electrode area, stretched tight, and sealed along all edges using 5-minute epoxy, completing the assembly of the cell.

Cell operation:

The electrochemical cell was connected to a flow system that included a gas sparging chamber and an HPLC pump (Scientific Systems, Inc.) that produced a flow of electrolyte over the catalyst surface (Figure S1). The HPLC pump features a built-in pulse damping system to provide steady liquid flow. The electrolyte flow rate was varied for different measurements, including no flow conditions and flow rates as high as 45 mL/min, which corresponds to ~ 1 m/s linear velocity over the electrode surface. Ar (Airgas, Ultra High Purity 5.0) regulated by a mass flow controller (MKS Instruments) at 20 sccm, flowed through a gas bubbler filled with 18 Mohm*cm resistivity H_2O and into the gas sparging chamber. The electrolyte in the gas sparging chamber was separated into two compartments by a Ni mesh: the compartment through which Ar was bubbled and the compartment in which the electrolyte from the cell outlet was pumped back into the sparging chamber. A chelating agent (Chelex 100) was used to remove metal impurities from the electrolyte and to limit impurities from depositing on the sample surface during operation.

During *in situ* measurements, the cell was operated in a three-electrode configuration using a Ag/AgCl reference electrode connected to the cell through a piece of tubing filled with electrolyte. Buffer solutions of K_2HPO_4 (Fluka Analytical TraceSELECT >99.999% trace metals basis), KH_2PO_4 (Fluka Analytical TraceSELECT >99.995% trace metals basis), K_2CO_3 (Aldrich 99.995 % trace metals basis),

$KHCO_3$ (Sigma-Aldrich, 99.95% trace metals basis), and $K_3[Fe(CN)_6]$ (Acros Organics 99+% for analysis) were used as the electrolyte.

X-ray Characterization:

In situ GIXAS and GIXRD were performed at beamline 11-2 at the Stanford Synchrotron Radiation Lightsource (SSRL) at SLAC National Accelerator Laboratory. The energy of incident X-rays at the Cu K-edge for GIXAS measurements was controlled with a Si (220) double-crystal monochromator calibrated by defining 8979 eV as the maximum of the first inflection point of the first derivative of a spectra collected using a 5 um Cu foil. The beam line has an energy resolution of $\Delta E/E \sim 1x10^{-4}$. Harmonic rejection and collimation of the beam was done with a Rh-coated silicon mirror set with a 15 keV cut-off. Focusing was done downstream of the monochromator with a toroidal silicon mirror and in-hutch slits to achieve a vertical focus of ~ 30 μm and a nominal spot width of 1 mm. For grazing angles below 0.5°, at 9 keV (Cu K-edge) through an aqueous electrolyte layer, this corresponds to an illuminated area of approximately 1 mm by 2.8 mm. For higher angles, the illuminated length is reduced as the cosec of the angle.

Energy resolved fluorescence signal for XAS was collected with a monolithic 100-element Canberra germanium detector mounted at a 90° angle to the incident beam. Photon energy was resolved and integrated with XIA DXP-XMAP digital photon processors. A Pilatus 100K area detector from Dectris was used to measure scattered X-ray intensity. The detector has 94,965 pixels (487 x 195) with a pixel size of 172 μm x 172 μm. A Huber two-circle goniometer independently controlled the grazing incidence angle and the angle of the Pilatus area detector for GIXRD measurements. The goniometer and Pilatus detector were used to control incidence angle, align samples, and collect XRD data. GIXRD data were collected using a photon energy of 10 keV (1.24 Å).

Scattering measurements were converted from two-dimensional Pilatus images to two-theta values by integrating pixel rows of the images. The integrated data was smoothed using a Savitzky-Golay filter and background corrected by subtracting the measured intensity collected at an incident angle of 0 degrees; one exception is the data shown in Figure 3b, which is presented without smoothing in order to

illustrate the signal to noise level of the raw data during high-current operation. GIXRD measurements were corrected for refraction as described below. Each XRD image required 8 seconds of acquisition time. XRD diffractograms shown in Figure 3 were averages of 3 images, for a total acquisition time of 24 seconds, while those in Figure 4 were averages of 20 images for a total acquisition time of 160 seconds.

XAS spectra were processed using the Athena and Sixpack software packages.[3] XAS spectra were normalized using the background subtraction and intensity normalization functions in Athena. Averages of several sequential spectra were used to increase the signal-to-noise ratio. XANES spectra required ~13 minutes of data collection, and three consecutive scans were averaged together for a total of 39 minutes. EXAFS spectra required ~27 minutes of data collection, and three consecutive scans were averaged together for a total of 80 minutes.

Data Analysis for Grazing Incidence Measurements:

Collecting measurements in a grazing incidence geometry introduces complexities into data analysis and interpretation which are often ignored in standard XAS or XRD experiments. In particular, self absorption in XAS and refraction in XRD must be considered. Self absorption arises in fluorescence-detected XAS when a large number of Cu atoms are probed along the X-ray beam path, such that changes in absorption coefficient as the X-ray energy is scanned can lead to changes in the X-ray path length through the sample.[4] For our GIXAS measurements, this effect is most pronounced at shallower grazing angles, and tends to reduce the relative intensity of the strongest spectral features (Figure S4). Therefore, the intensity ratios of major spectral features vary with grazing angle, even for fully reduced metallic copper. The large self-absorption effect prohibits a quantitative fit using standard spectra measured as ex-situ samples; hence, the thickness of the oxide layer cannot be calculated without a rigorous self-absorption correction. Existing correction algorithms do not consider grazing incidence X-ray beam paths and are therefore insufficient.[4-6] While a new correction scheme for grazing incidence geometries is under development, it is beyond the scope of this manuscript. We note, however, that relative energy positions of spectral features still allow for meaningful interpretation of spectra. Even without quantitative analysis, the signatures of Cu (I) on the surface at OCP are clear.

In order to make a rough estimate of the thickness of the Cu(I) layer, we apply a simple self-absorption correction during our difference spectrum analysis described in the main text. The correction uses the ratio of the 0.15° surface spectrum at -0.5 V vs. RHE to the Cu foil standard spectrum, under the assumption that the thin film surface at -0.5 V vs. RHE is fully reduced metallic Cu, and therefore any intensity differences between its spectrum and that of the Cu foil standard are solely due to self-absorption effects. Using this ratio as a multiplicative factor for the sample difference spectrum allows us to compare the sample difference spectrum and standard difference spectrum as shown in Figure 4b in the main text. Scaling the corrected sample difference spectrum by a factor of 3 results in a good match to the standard difference spectrum, which implies that the Cu(I) layer on the thin film surface at OCP contributes 1/3 of the total XANES signal. This corresponds to a thickness of ~1-2 nm. We stress that this is a rough estimate and that a full quantitative analysis requires more rigorous self-absorption corrections as discussed above.

In GIXRD, the refraction of X-rays entering the electrolyte in the cell must be considered. In this work, all XRD measurements are corrected for refraction using a modified version of a previous correction to account for the refractive index of the aqueous electrolyte.[7] This modified version will be described in an upcoming manuscript. The effect of refraction can be clearly seen in our XRD measurements (Figure S5). Before correction, the Cu (111) peak position seems to shift as a function of incidence angle. After correcting for refraction, however, the Cu (111) peak appears at the same two-theta position throughout the range of angles tested (Figure 4e). This correction is vital for determining the position of a peak in grazing incidence X-ray diffraction.

Calculation of Boundary Layer Thickness

Fick's first law can be written as

$$J = -D\frac{\partial \varphi}{\partial x}$$

where J is the diffusional flux (mol*m^{-2}*s^{-1}), D is the diffusion coefficient (m^2*s^{-1}), φ is the concentration (mol*m^{-3}), and x is the dimension of diffusion (m). We approximate the diffusional gradient as being linear, giving

$$J = -D\frac{\Delta \varphi}{\Delta x}$$

Defining the boundary layer thickness, δ, as the distance from the electrode at which the concentration of the reactant at a steady state current is equal to the bulk concentration of the reactant, we can write

$$J_{SS} = -D\frac{\varphi_0}{\delta}$$

where J_{SS} is the steady-state diffusional flux in the diffusion limited current regime and φ_0 is the bulk concentration of the reactant. Rearranging this equation and including Faraday's constant F (96485 C*mol^{-1}) allows the boundary layer thickness to be written in terms of the steady state current density, j_{SS} (C*s^{-1}*m^{-2})

$$\delta = -D\frac{\varphi_0 * F}{j_{SS}}$$

A value of 7.26*10^{-6} cm^2*s^{-1} was used for the diffusion coefficient of potassium ferricyanide in this work.[8]

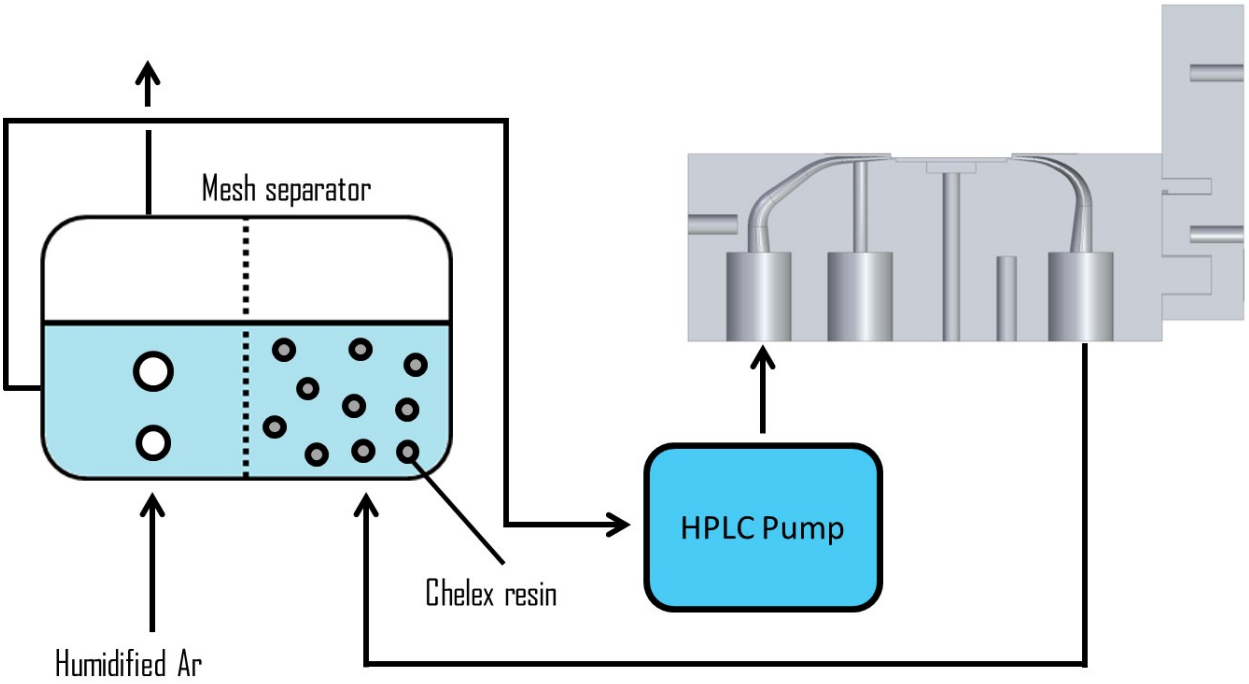

Figure S1: Schematic of the liquid flow system used in the grazing incidence XAS / XRD experiments. Electrolyte is sparged with humidified Ar before entering a pulse-dampened HPLC pump (SSI) which feeds the electrolyte to the electrochemical cell. After passing through the cell, electrolyte flows through a chamber loaded with Chelex resin to remove any trace metal contaminants before passing through a mesh separator and entering the sparge chamber again.

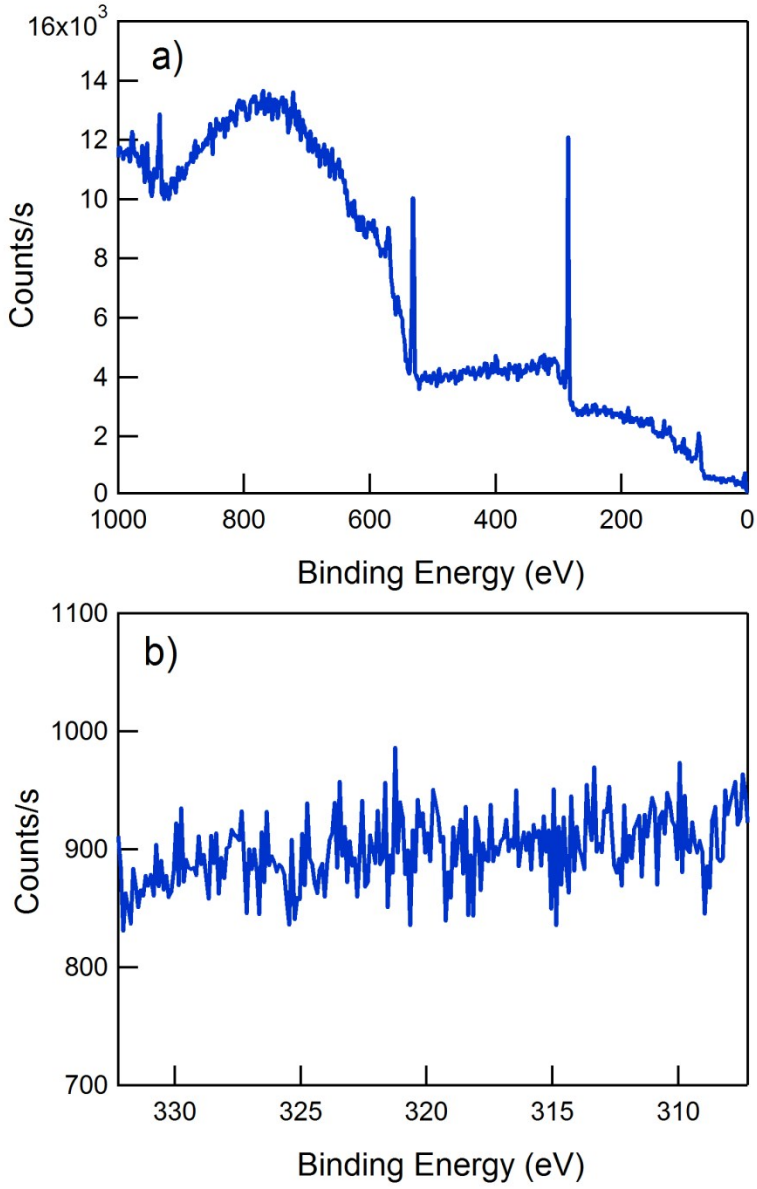

Figure S2: X-ray photoelectron spectroscopy (XPS) of the Cu electrode characterized in Figure 3, following testing at -1.1 V vs. RHE in Ar sparged, 0.1 M pH 6.8 potassium phosphate electrolyte. **a).** Survey XPS scan showing peaks characteristic of Si (100 eV), P (133 eV, from phosphate electrolyte), C (285 eV), O (532 eV), and Cu (933 eV). No evidence of Pt or other metal contaminants is seen. **b).** High resolution XPS scan of Pt 4d region, showing no sign of Pt contamination.

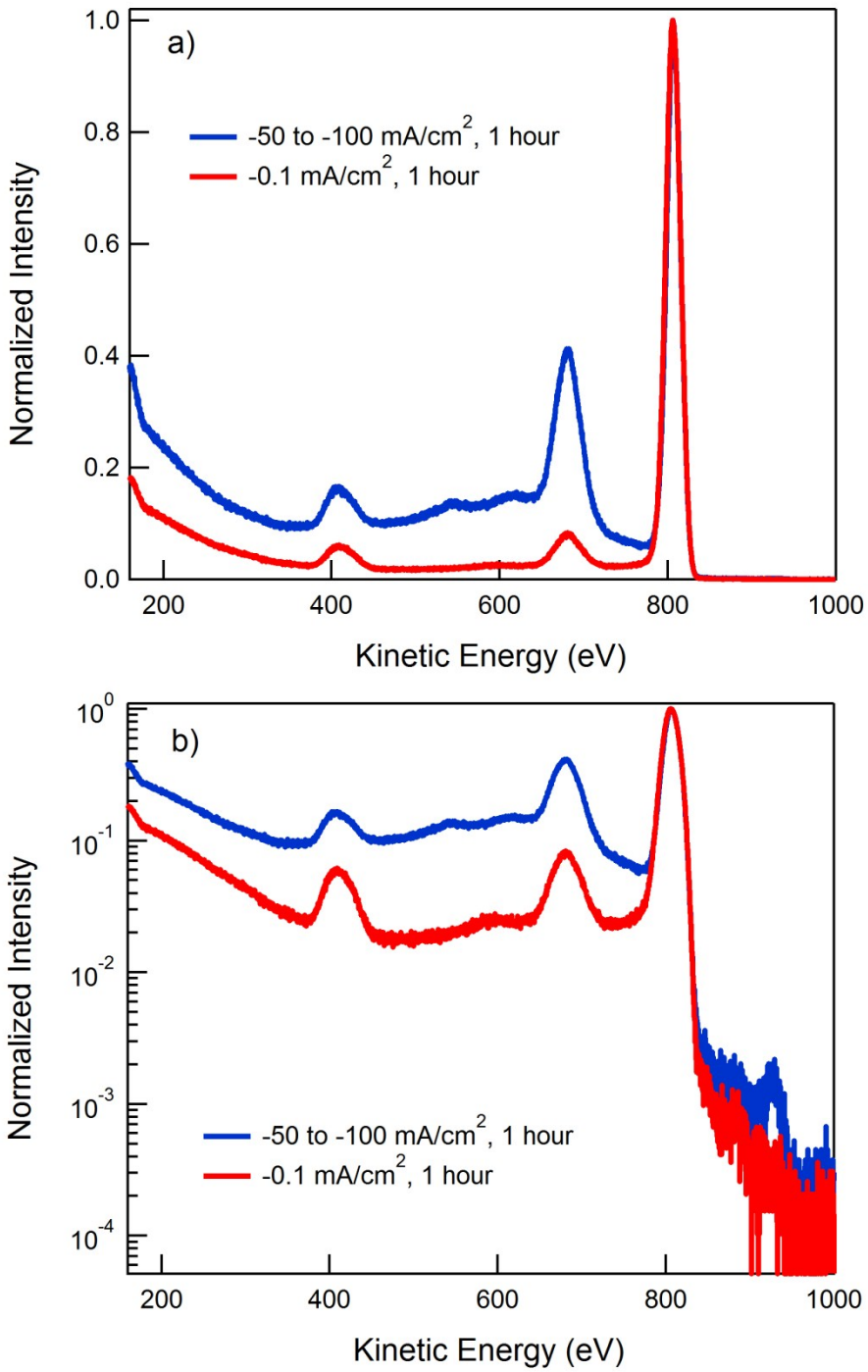

Figure S3: Post-reaction low-energy ion scattering (LEIS) spectra of thin-film Cu electrodes tested under low (-0.1 mA/cm^2, red) and high (-50 to -100 mA/cm^2, blue) current density conditions, plotted with a linear (top) and logarithmic (bottom) intensity scale. Peaks at ~410 eV, ~680 eV and ~805 eV correspond to O, K, and Cu, respectively. Smaller peaks at ~545 eV and ~615 eV correspond to Na and Si, respectively In the logarithmic plot, a small peak at ~928 eV corresponding to Pt (from the counter electrode) can be seen. The low intensity of this peak indicates that the Chelex is effective at removing trace metal contaminants from the flow system, even during high current density operation.

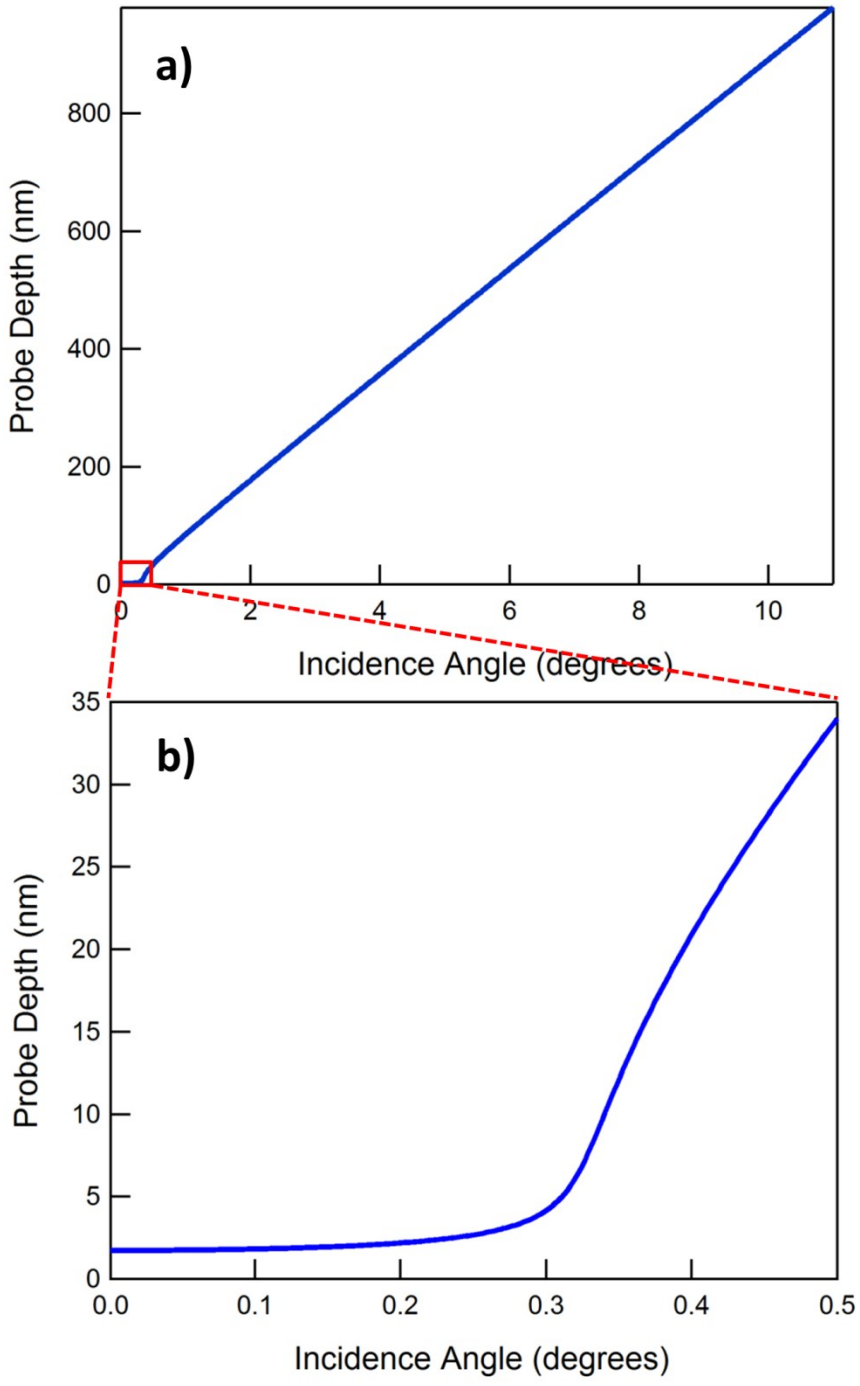

Figure S4: Calculated probe depth of 10 keV X-rays into Cu as a function of incidence angle. **a)** The full range of incidence angles from 0 to 11 degrees, indicating a maximum probe depth of nearly 900 nm. **b)** Enlarged plot of the area indicated by a red box in panel a. Incidence angles between 0.1 and 0.3 degrees probe ~2-4 nm of the sample surface. Calculations use data tables from literature.

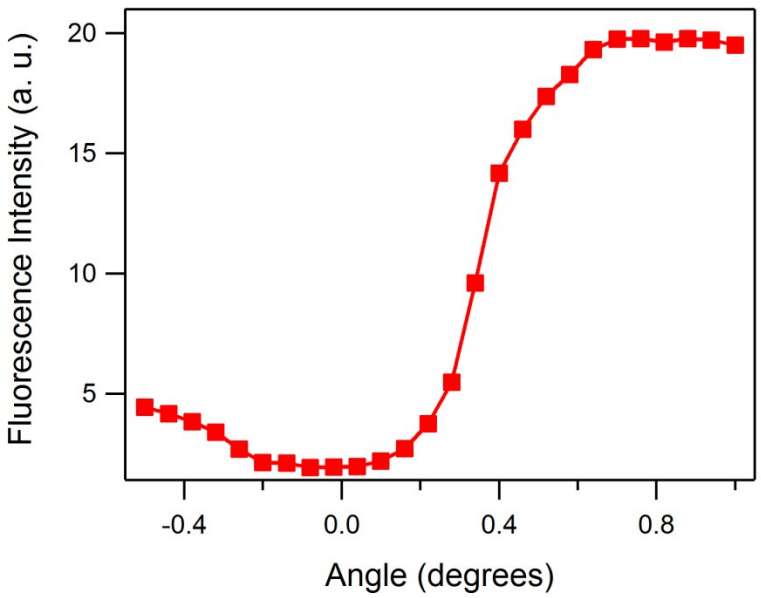

Figure S5: Measured angle curve for a Cu thin-film sample at open circuit in 0.1 M potassium carbonate, using Cu K-edge fluorescence intensity as a function of incidence angle for 10 keV X-rays.

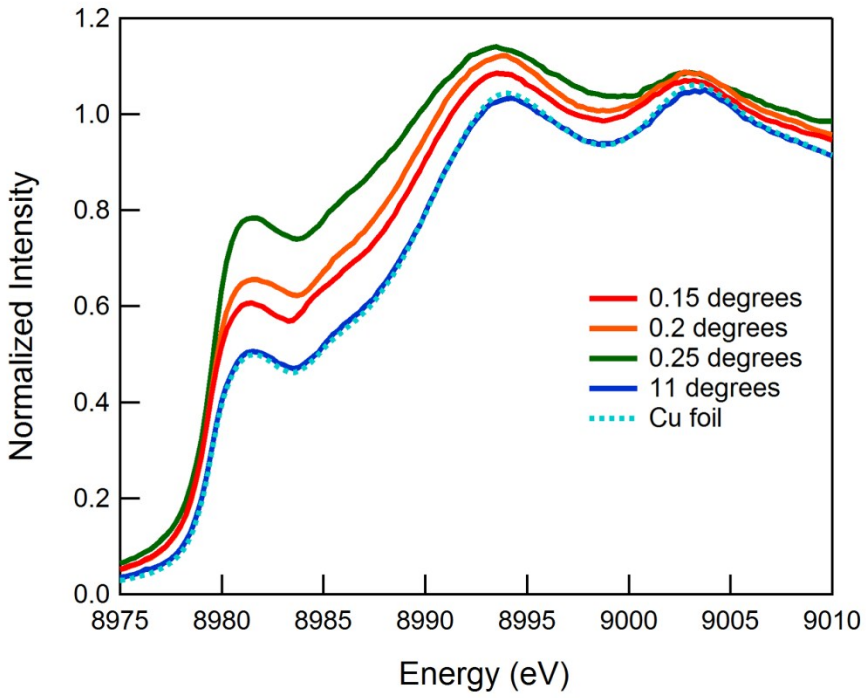

Figure S6: XANES spectra as a function of incidence angle (and therefore probe depth) for a Cu sample in a 0.1 M, pH 10 potassium carbonate buffer, held at -0.5 V vs. RHE, with a Cu foil reference spectrum for comparison. The XANES at 11 degrees closely matches the Cu foil spectrum, while the others match the peak positions but have anomalous spectral intensity due to angle-dependent self-absorption effects.

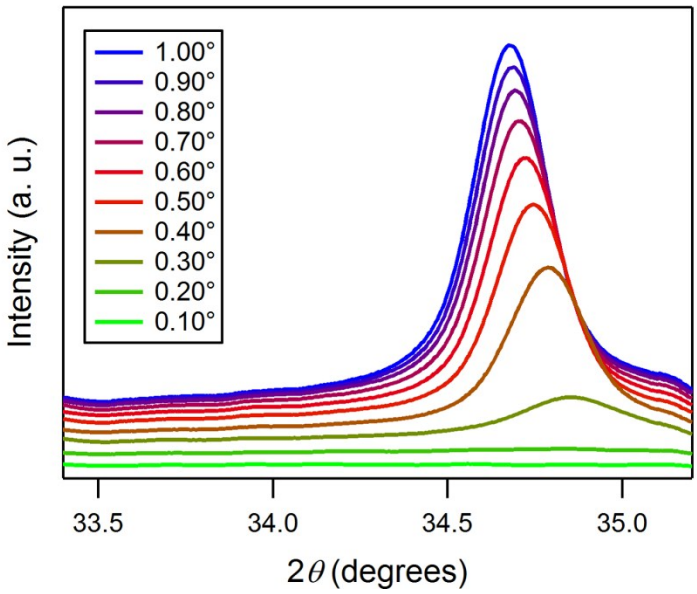

Figure S7: GIXRD at various incidence angles of a thin film Cu electrode at the OCP in a 0.1 M, pH 10 potassium carbonate buffer solution before refraction correction. Without refraction correction, a clear shift in peak position is observed as a function of incidence angle. Following refraction correction, the peak position aligns at all incidence angles as shown in Figure 4e in the main text.

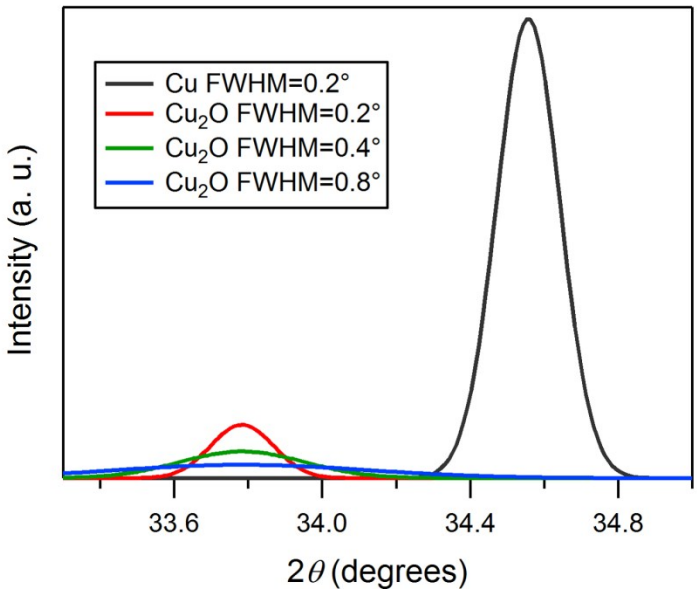

Figure S8: Calculations to estimate the feasibility of observing a relatively disordered Cu_2O peak. A 2:1 Cu to Cu_2O ratio is used as described in the main text. A FWHM of 0.2 degrees is chosen for the Cu (111) peak to match the width observed experimentally. The Cu_2O peak needs to be approximately four times as wide as the Cu peak not to be observed in the experimental GIXRD measurements, suggesting the Cu_2O is at least four times as disordered as the metallic Cu. Calculations were performed using Powdercell.[9]

References

1. C. Hahn, T. Hatsukade, Y.-G. Kim, A. Vailionis, J. H. Baricuatro, D. C. Higgins, S. A. Nitopi, M. P. Soriaga and T. F. Jaramillo, *Proc. Natl. Acad. Sci.*, 2017, **114**, 5918-5923.
2. C. Hahn, D. N. Abram, H. A. Hansen, T. Hatsukade, A. Jackson, N. C. Johnson, T. R. Hellstern, K. P. Kuhl, E. R. Cave, J. T. Feaster and T. F. Jaramillo, *J. Mater. Chem. A*, 2015, **3**, 20185-20194.
3. B. Ravel and M. Newville, *J. Synchrotron Radiat.*, 2005, **12**, 537-541.
4. P. Pfalzer, J. P. Urbach, M. Klemm, S. Horn, M. L. denBoer, A. I. Frenkel and J. P. Kirkland, *Phys. Rev. B*, 1999, **60**, 9335-9339.
5. C. H. Booth and F. Bridges, *Phys. Scr.*, 2005, **2005**, 202.
6. L. Tröger, D. Arvanitis, K. Baberschke, H. Michaelis, U. Grimm and E. Zschech, *Phys. Rev. B*, 1992, **46**, 3283-3289.
7. M. F. Toney and S. Brennan, *Phys. Rev. B*, 1989, **39**, 7963-7966.
8. S. J. Konopka and B. McDuffie, *Anal. Chem.*, 1970, **42**, 1741-1746.
9. W. Kraus and G. Nolze, *J. Appl. Crystallogr.*, 1996, **29**, 301-303.